Journal of Membrane Science Letters 4 (2024) 100067

Contents lists available at ScienceDirect

Journal of Membrane Science Letters

journal homepage: www.elsevier.com/locate/memlet

Chemically recyclable nanofiltration membranes fabricated from two circular polymer classes of the same monomer origin

Rifan Hardian [a], Abdul Ghaffar [a], Changxia Shi [b], Eugene Y.-X. Chen [b], Gyorgy Szekely [a,c,*]

[a] Advanced Membranes and Porous Materials Center, Physical Science and Engineering Division, King Abdullah University of Science and Technology (KAUST), Thuwal, 23955-6900, Saudi Arabia
[b] Department of Chemistry, Colorado State University, Fort Collins, CO 80523-1872, USA
[c] Chemical Engineering Program, Physical Science and Engineering Division, King Abdullah University of Science and Technology (KAUST), Thuwal, 23955-6900, Saudi Arabia

ARTICLE INFO

Keywords:
Nanofiltration
Polyester
Poly(cyclic olefin)
Green solvent
Recyclable polymer
Circular economy

ABSTRACT

Nanofiltration is widely used in various industries to separate solutes from solvents. To foster a circular economy, establishing a closed-loop lifecycle for the membrane materials is highly important. In this study, we fabricated recyclable nanofiltration membranes from chemically recyclable polymers —polyester $P(BiL^{=})_{ROP}$ and poly (cyclic olefin) $P(BiL^{=})_{ROMP}$— using γ-butyrolactone as a green solvent. These two polymers, of two different polymer classes, were obtained from a single monomer, which could be recycled back to the same monomer, exhibiting the unique "one monomer–two polymers–one monomer" closed-loop chemical circularity. The effect of physical treatment, such as annealing, hot-pressing, and air exposure on the morphological characteristics and performance of the nanofiltration membranes was investigated. We revealed the interplay between membrane pore size, thickness, density and the molecular sieving performance of the nanofiltration membranes. Solute rejections were mainly governed by the membrane pore size. However, solvent flux was mainly governed by the membrane density that determines the free volume interconnectivity. The membranes exhibited a tunable molecular weight cutoff between 553 and 777 g mol^{-1} and methanol permeance between 5.9 and 9.8 L m^{-2} h^{-1} bar^{-1}. The membranes exhibited excellent long-term nanofiltration stability over 1 week. The combination of the green solvent used for membrane fabrication and the circular life cycle of the polymer membrane brings one step closer to closing the circularity loop of membrane technology.

1. Introduction

Chemical separation accounts for the majority of global industrial energy consumption (Sholl and Lively, 2016). In particular, many sectors including the pharmaceutical, fine chemical, petrochemical, food, and textile industries use organic solvents in their production (Clarke et al., 2018). To separate solutes from solvents, membrane-based separation processes are considered more energy-efficient than conventional thermal-based separation such as cryogenic distillation (Datta et al., 2022). In organic solvent nanofiltration (OSN) process, pressure is applied through a membrane to separate solutes of molecular weights between 100 and 2000 g mol^{-1} from either polar or nonpolar organic solvents.

At present, most nanofiltration membranes are fabricated from petroleum-derived polymers, such as polybenzimidazole, poly(dimethylsiloxane), polysulfone, and polyamide, raising sustainability concerns (Hardian et al., 2021; Serbanescu et al., 2020; Tan et al., 2018; Zakharova et al., 2021). Moreover, these polymers are typically processed using toxic and hazardous organic solvents, such as *N,N*-dimethylacetamide (DMAc), *N,N*-dimethylformamide (DMF), and *N*-methyl-2-pyrrolidinone (NMP), which pose a series of health and environmental risks (Belfort, 2019; Cheng et al., 2018; Nunes et al., 2020). The importance of employing green solvents in polymer membrane fabrication has been emphasized in recent studies (Hessel et al., 2021; Xie et al., 2021; Zou et al., 2021). Moreover, nanofiltration membranes fabricated from these conventional polymers typically

Web: https://www.SzekelyGroup.com
* Corresponding author.
E-mail address: gyorgy.szekely@kaust.edu.sa (G. Szekely).
@SzekelyGroup (G. Szekely)

https://doi.org/10.1016/j.memlet.2024.100067
Received 31 December 2023; Received in revised form 19 January 2024; Accepted 20 January 2024
Available online 28 January 2024

undergo a linear life cycle, which end up in a landfill or incinerated (Li et al., 2023). Design thinking toward end-of-life and waste management of the membranes and their processes is necessary to address the health, safety, and environmental concerns (Figoli et al., 2014; Kim and Nunes, 2021; Xie et al., 2021). Therefore, it is important to explore alternative polymers that can ensure minimum dependency on nonrenewable petroleum-based polymer materials, and could benefit waste management from an economic perspective (Kim and Nunes, 2021; Syeda et al., 2022). Such polymers must ideally be recyclable, sourced from renewable sources, and processable using green solvents.

Sustainable nanofiltration membranes are fabricated to promote environmental health and conservation, in line with the United Nations' Sustainable Development Goals, and achieve clean water and sanitation, affordable and clean energy, climate action, and aquatic life below water (Ogunmakinde et al., 2022; Syeda et al., 2022). Sustainable nanofiltration membranes can be classified based on the employed solvents and the membrane materials (Nguyen Thi et al., 2021). Based on the employed solvents, the selection of green solvents that can be used to fabricate nanofiltration membranes are provided in the list of GSK's solvent sustainability guide (Alder et al., 2016), which considers the lifecycle impact, health, environment, safety, and waste categories. Some examples on the use of biobased polymers for nanofiltration and other membranes have been reported in the literatures, which includes the use of cellulose derivatives, algal biomass and polyesters (Fatima et al., 2023; Hardian et al., 2022; Rasool and Vankelecom, 2021; Tomietto et al., 2022; Tran and Ulbricht, 2023; Yang et al., 2023). In these literatures, the membranes were fabricated via phase inversion technique using green solvents, and the bio-sourced polymer solutions were cast on the nonwoven polypropylene support to enhance their mechanical stability. Despite addressing as many green chemistry and engineering principles as possible, the use of polypropylene supports is undesired because it is sourced from petrochemical derivatives.

Herein, we fabricated free-standing recyclable nanofiltration membranes with remarkable mechanical stability from novel polyester P(BiL$^{=}$)$_{ROP}$ and poly(cyclic olefin) P(BiL$^{=}$)$_{ROMP}$ polymers using γ-butyrolactone as the green solvent (Fig. 1). Importantly, both polymers were originated from a single hybrid bicyclic lactone-olefin (BiL$^{=}$) monomer, a hybridization of γ-butyrolactone and cyclohexene constituents. These two constituents and their derivatives can be extracted from natural products and biologically synthesized, making them categorized into renewable sources. For instance, γ-butyrolactone can be derived from succinic acid obtained from anaerobic metabolism during microbial fermentation (Caretto et al., 2014; Lee et al., 2011). Moreover, cyclohexene and its derivative can be found in small Japanese tree *Lindera umbellata* and L. *umbellata vat. lancea* (Gribble, 1991). The BiL$^{=}$ monomer underwent ring-opening polymerization (ROP) and ring-opening metathesis polymerization (ROMP) to generate P(BiL$^{=}$)$_{ROP}$ (a class of polyester) and P(BiL$^{=}$)$_{ROMP}$ (a class of poly(cyclic olefin)), respectively (Shi et al., 2022). Both polymers can be depolymerized back to the same monomer in the presence of a catalyst, thereby allowing the recovery of their constituent monomer BiL$^{=}$on demand, promoting sustainable end-of-life cycle and a circular plastic economy. The properties and nanofiltration performance of the membranes were investigated in depth. The interplay between the membrane pore size, density, and thickness with their nanofiltration performance was evaluated.

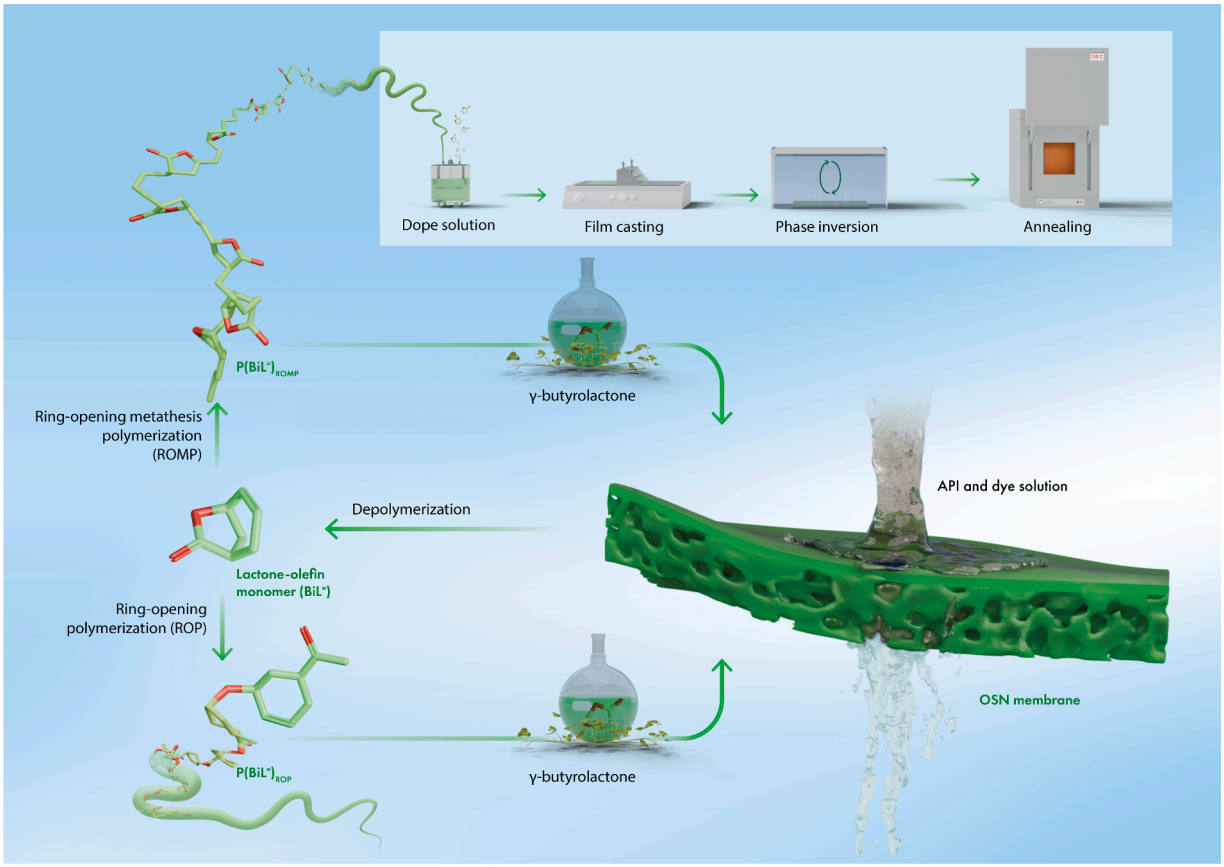

Fig. 1. Sustainable lifecycle of recyclable "one monomer–two polymers–one monomer" membranes for organic solvent nanofiltration (OSN): ring-opening polymerization (ROP) and ring-opening metathesis polymerization (ROMP) of hybrid lactone-olefin monomer that yielded P(BiL$^{=}$)$_{ROP}$ and P(BiL$^{=}$)$_{ROMP}$ polymer structures (see also Scheme S1); both polymers can be fabricated into OSN membranes using γ-butyrolactone green solvent. Membrane fabrication; the dope solution containing polymer and green solvent is cast, and the formed film is immersed in a water coagulation bath followed by annealing.

2. Results and discussions

2.1. Membrane fabrication strategy

The membrane fabrication strategy involved solvent selection, viscosity determination, and membrane post-treatment. To identify a suitable solvent to process P(BiL$^{=}$)$_{ROP}$ and P(BiL$^{=}$)$_{ROMP}$ polymers into membranes, several green and conventional solvents were tested to solubilize the polymers (Table S1). From 42 solvents, the P(BiL$^{=}$)$_{ROP}$ polymer was soluble in 16 green and 9 conventional solvents. However, only 8 green and 6 conventional solvents were able to dissolve the P(BiL$^{=}$)$_{ROMP}$ polymer. The limited solubility of P(BiL$^{=}$)$_{ROMP}$ could be due to its higher number-average molecular weight (M_n = 162.4 kDa) than that of P(BiL$^{=}$)$_{ROP}$ (M_n = 84.4 kDa). Moreover, the rigid structure of P(BiL$^{=}$)$_{ROMP}$ owing to the introduction of C=C in the backbone possibly contributed to the enhanced solvent-resistant property.

Water was selected as the coagulation media during phase inversion for membrane fabrication because it is the greenest solvent, abundantly available, and economically feasible. Among all the green solvents that could dissolve both P(BiL$^{=}$)$_{ROP}$ and P(BiL$^{=}$)$_{ROMP}$, only 4 were miscible with water: dimethyl isosorbide, PolarClean, γ-butyrolactone, and γ-valerolactone. The boiling point of dimethyl isosorbide (95 °C) is very close to that of water (100 °C); thus, it could pose a challenge in the potential recovery of solvents via distillation. In contrast, PolarClean (boiling point: 282 °C) exhibited low polymer solubility (maximum of 18 wt% and 5 wt% for P(BiL$^{=}$)$_{ROP}$ and P(BiL$^{=}$)$_{ROMP}$). Due to structural similarity with the polymers, γ-butyrolactone (boiling point: 204 °C) was selected as the appropriate solvent because it showed the highest polymer solubility (>30 and 6.5 wt% for P(BiL$^{=}$)$_{ROP}$ and P(BiL$^{=}$)$_{ROMP}$).

We determined the polymer dope solution concentration to reach adequate viscosity for casting. In general, three concentration regions could be distinguished in the concentration versus viscosity curve, namely, dilute, semidilute, and concentrated regions (Strivens, 1999), as shown in Fig. S1. The viscosity was considerably low in the dilute region, resulting in a very thin membrane with poor mechanical properties. However, it was substantially high in the concentrated region, resulting in a very thick membrane that limited permeation. Adequate viscosity for casting was achieved in the semidilute concentration region, indicated in the inflection region in the concentration versus viscosity curve. The semidilute concentration was obtained at 30 and 6.5 wt% of P(BiL$^{=}$)$_{ROP}$ and P(BiL$^{=}$)$_{ROMP}$, with 4660 and 4280 mPa s viscosities, respectively (Fig. S2a). Both polymers exhibit different viscosities because they have different structures and respond differently to three intermolecular forces, i.e., between the polymer molecules, between the solvent molecules, and between the polymer and solvent molecules (Strivens, 1999).

The dope solutions were cast, followed by phase inversion in water to form free-standing membranes. The morphologies of the resulting membranes were characterized via scanning electron microscopy (SEM) as shown in Fig. S2b–i. Both P(BiL$^{=}$)$_{ROP}$ and P(BiL$^{=}$)$_{ROMP}$ membranes exhibited typical integrally skinned asymmetric morphology at the cross-section, with a thin layer on the top region and finger-like macrovoids in the bottom region of the membranes. The P(BiL$^{=}$)$_{ROP}$ membrane was approximately three times thicker than the P(BiL$^{=}$)$_{ROMP}$ membrane because the concentration of P(BiL$^{=}$)$_{ROP}$ dope solution was approximately five times higher than that of the P(BiL$^{=}$)$_{ROMP}$ dope solution. The P(BiL$^{=}$)$_{ROP}$ membrane surface had a pore size of ~40 nm (Fig. S2c), which is considerably large for nanofiltration applications. However, the P(BiL$^{=}$)$_{ROMP}$ exhibited considerably larger voids (up to 12 μm), indicative of a defective membrane (Fig. S2f). To reduce the membrane pore sizes, the cast solution was exposed to air before the membranes were immersed in water. After 30 mins of exposure, the P(BiL$^{=}$)$_{ROP}$ membrane surface showed a smooth and homogenous morphology without any observable porosity (Fig. S3). However, P(BiL$^{=}$)$_{ROMP}$ membrane exhibited observable surface porosity (~200 nm size) even after 0.5 h of exposure to air before coagulation in water (Fig. S4). Additionally, the membranes were annealed at various temperatures to reduce their pore sizes. The P(BiL$^{=}$)$_{ROP}$ membrane did not present any observable surface porosity after annealing at 120 °C for 2 h (Fig. S5). Meanwhile, P(BiL$^{=}$)$_{ROMP}$ exhibited relatively large surface porosity (Fig. S6) after annealing under the same thermal conditions. As the P(BiL$^{=}$)$_{ROMP}$ membrane defects could not be eliminated, only the P(BiL$^{=}$)$_{ROP}$ membrane was characterized further because it showed good membrane-forming ability with potential application for nanofiltration. Indeed, P(BiL$^{=}$)$_{ROP}$ and P(BiL$^{=}$)$_{ROMP}$ were successfully fabricated as dense films (Fig. S7), which can potentially be used for gas separation. However, this is out of the scope of this study.

2.2. Membrane characterization and recyclability

The membrane designation is presented in Table 1, and the effect of annealing, hot-pressing, and air exposure on the membrane properties are presented in Fig. 2. From differential scanning calorimetry (DSC) analysis (Fig. 2a), the endothermic peak at around 108 °C was observed in both the polymer and the membrane, which corresponds to the glass transition temperature (T_g) of P(BiL$^{=}$)$_{ROP}$. Interestingly, an exothermic peak at around 196 °C was only observed in the membrane, but it was not observed in the polymer. This exothermic peak was likely a result of physical crosslinking of the double bonds (exothermic reaction) that occurred during membrane preparations. Physical crosslinking is the formation of bonds between polymer chains through weak interactions (such as coordination bonding, hydrogen bonding, ionic interactions, and van der Waals interactions). Whereas, chemical crosslinking occurs through the formation of covalent bonding, which is facilitated by the addition of crosslinking agents (Dodero et al., 2021; Hu et al., 2019; Rebers et al., 2021). As the membranes were prepared without the addition of crosslinking agents, only physical crosslinking may occur. When the polymers were dissolved and coagulated during membrane fabrication, the polymer chain entanglements were altered. The rearrangement of the polymer chains modified the hydrogen bonding and van der Waals interactions between the polymers chains, which induced physical crosslinking.

M2 was prepared by heating M1 at 120 °C for 2 h. Above its glass transition temperature (~108 °C), the polymer structure changed gradually from a hard and relatively brittle state to a rubbery state, which enable the polymer rearrangement. The thermal property of M1 and M2 were very similar, where both M1 and M2 showed T_g at the same temperature regions (Fig. 2b). M3 was prepared by sandwiching M1 between two glass plates (hot-pressing) and heating at 120 °C for 2 h. Similar to M2, the thermal property of M3 remains unchanged (Fig. 2b). M4, prepared by exposing the cast solution in air for 30 min prior to water coagulation, also exhibited similar thermal properties as M1, M2, and M3. The exothermic peaks were observed in a relatively narrow temperature range, between 185 and 195 °C (Fig. 2b). A slight shift in the exothermic peak could be attributed to the different modification treatments employed to different membranes, which influenced the physically crosslinked structures of the polymers. Thermogravimetric analysis (TGA) curves of M1–M4 showed the same thermal profiles with a sharp degradation temperature at ~258 °C (Fig. 2c). The Fourier transform infrared (FTIR) spectra of the gas released when heating M1

Table 1
Membrane designations: free standing P(BiL$^{=}$)$_{ROP}$ membranes fabricated using 30 wt% dope solution in γ-butyrolactone followed by casting (200-μm knife thickness) and coagulating in water; n.a. = not applicable.

Membranes (-)	Evaporation time (min)	Heating temperature (°C)	Heating time (h)	Hot-pressing (-)
M1	0	n.a.	n.a.	no
M2	0	120	2	no
M3	0	120	2	yes
M4	30	n.a.	n.a.	no

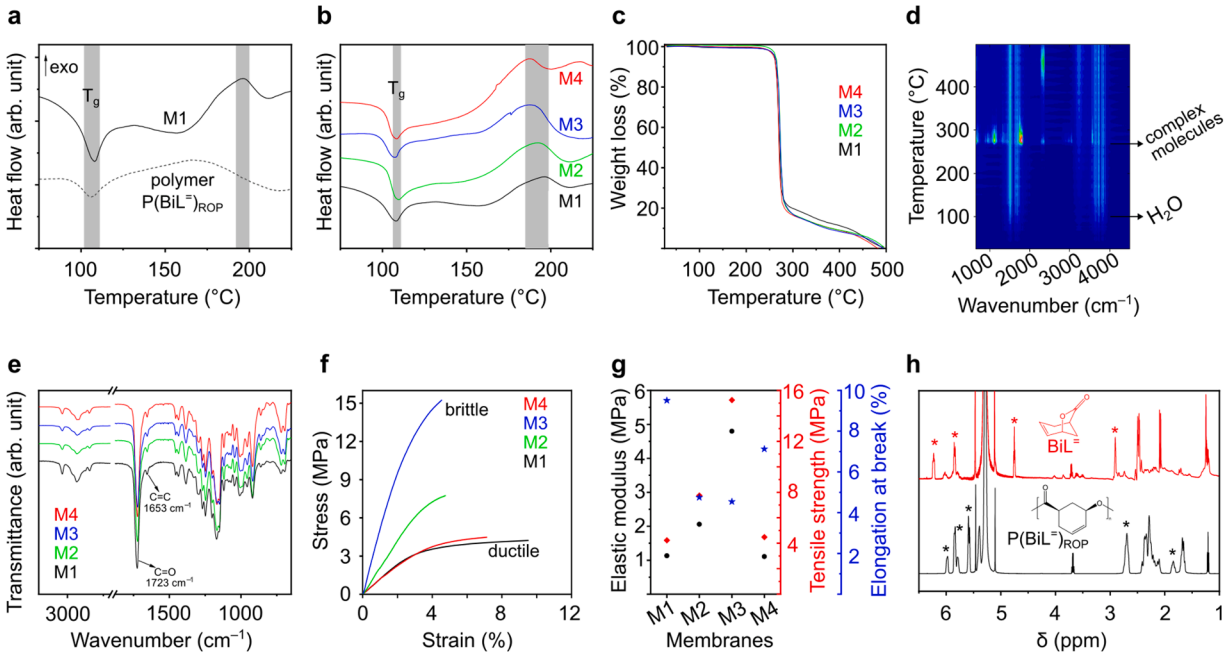

Fig. 2. Differential scanning calorimetry (DSC) curve of M1 membrane (solid line) and $P(BiL^{=})_{ROP}$ polymer (dotted line) from room temperature to 250 °C (a); DSC (b) and thermogravimetric analysis (TGA) (c) curves of M1–M4; FTIR spectra of the gas released during the thermal analysis of M1–M4 (d); FTIR spectra of M1–M4 (e); stress–strain curve (f) and mechanical properties (g) of M1–M4; ^{1}H NMR spectra (f) of M1 before (black) and after (red) depolymerization.

(Fig. 2d) showed two species. At 100 °C, weak FTIR signals corresponding to water adsorbed on the membrane surface were identified at 1700 and 3600 cm^{-1}. More complex FTIR signals were identified at 258 °C, corresponding to the complete degradation of the polymers.

The FTIR spectra of M1–M4 are identical (Fig. 2e), indicating that the pristine (M1) and physically treated (M2–M4) membranes had similar chemistry. The $P(BiL^{=})_{ROP}$ structure showed νC=C from the cyclohexene form at 1653 cm^{-1} and C=O stretching at 1723 cm^{-1}. In contrast, the mechanical behaviors of the membranes were distinct, as shown in the strain–stress curves (Fig. 2f). M1 and M4 showed a more ductile characteristic, whereas the thermally treated M2 and M3 showed a more brittle characteristic. After heating to 120 °C, the elastic modulus and tensile strength of M2 increased from 1.13 to 2.06 MPa and from 4.23 to 7.74 MPa, respectively, whereas its elongation at break reduced from 9.51% to 4.75% (Fig. 2g). The elastic modulus and tensile strength of M3 further increased to 4.79 and 15.24 MPa, respectively. Meanwhile, the elastic modulus and tensile strength of M4 were quite similar to M1 at 1.11 and 4.48 MPa, respectively. These observations indicated that thermal treatment induced rigidity in the polymer and reduced its plasticity.

To promote a sustainable end-of-life treatment of the fabricated membranes, M1 was depolymerized using a catalyst, $ZnCl_2$. The proton NMR spectra of M1 derived from $P(BiL^{=})_{ROP}$ polymer and its depolymerized $BiL^{=}$ monomer are shown in Fig. 2h. The $P(BiL^{=})_{ROP}$ membrane was successfully transformed back to its monomer, confirming its recyclability and enabling its usage for other applications. The detail assignments of the NMR peaks are provided in Fig. S8. The treated membranes (M2 and M3) and also the membranes that have been used for OSN test exhibited excellent recyclability to their parent monomers (Fig. S10). These findings were crucial because we can fine-tune the molecular sieving properties of the membranes via various physical treatments without compromising monomer recycling.

The surface of M1 membrane exhibited observable pores of approx. 40 nm size (Fig. 3a), which could be tightened by heating at 120 °C (Fig. 3b) and hot-pressing (Fig. 3c). Additionally, the large pores on the membrane surface of M1 were also successfully eliminated, after the cast solution was exposed to air for 30 mins prior to water coagulation (M4).

The tightening of the surface porosity was also confirmed by the atomic force microscopy (AFM) images where the observable pores in M1 surface (Fig. 3i) were absent in M2 (Fig. 3j) and M3 (Fig. k) surfaces. The cross-sectional images of M1–M3 displayed integrally skinned asymmetric structure, except that a denser morphology with thinner membrane thickness was clearly observed for M3. These observations indicated that heating process induced pore closure on the surface which caused a slight increase in the density from 0.46 to 0.58 g cm^{-3} (Fig. 3k–l). Whereas, due to the combined effects of mechanical pressure and heating during hot-pressing, densification occurred in both surface and cross-section of the membrane, considerably increasing the density from 0.46 to 0.76 g cm^{-3} (Fig. 3k and 3m). The cross-sectional morphology of M4 was distinct from M1–M3; its macrovoid size was considerably smaller and more compact than those in M1–M3. The morphology of M4 yielded a density of 0.64 g cm^{-3}, higher than those of M1 and M2 but lower than that of M3. The water contact angles of M1–M4 were relatively similar (61°–68°), indicating that the hydrophilic characteristics originated from the ketone and ether functional groups in the $P(BiL^{=})_{ROP}$ structure. In conclusion, physical treatments (annealing, hot-pressing, and air exposure) did not alter the chemical and thermal properties of the membranes but affected their morphology and mechanical properties.

2.3. Nanofiltration performance

The membrane separation performance was evaluated for OSN. The membranes demonstrated excellent stability in water, hexane, heptane, acetonitrile, and various alcohols. All the tested solutes with various molecular weights (236–1017 g mol^{-1}) passed through M1 with negligible rejections (Fig. 4a), which indicates the presence of large porosity on the membrane surface, as observed in the SEM images (Fig. 3a). The list of tested solute molecules is given in Table S2. M2–M4 membranes exhibited considerable rejection curves with various molecular weight cutoff (MWCO) values. The heating process in M2 resulted in a membrane with MWCO value of 624 ± 27 g mol^{-1} which correspond to the membrane pore radius of 0.72 nm (Fig. 4b). Meanwhile, the hot-pressing process in M3 tightened the MWCO value to 553 ± 28 g mol^{-1}, which

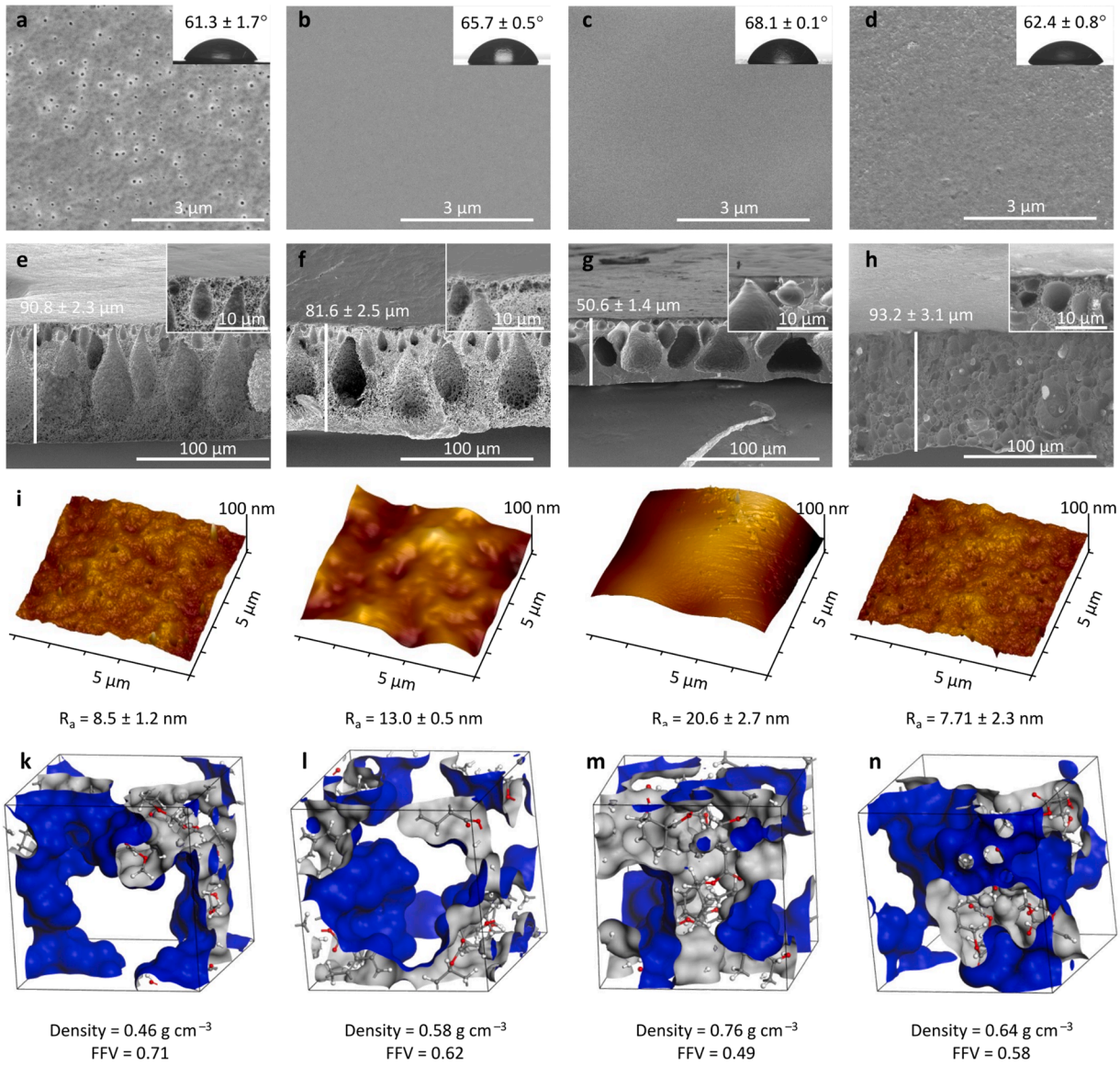

Fig. 3. SEM surface (a–d) and cross-section (e–h) images of M1, M2, M3, and M4; insets in Figs. 3a–3d indicate the water contact angles of membranes; 3D AFM topography (i–l) and fractional free volume (FFV) (k–n) of M1–M4. FFV was determined by using the Materials studio software: amorphous cell module was built from 10 chains length with benzyl alcohol as terminator, using the COMPASS II force field and experimentally measured density.

correspond to the membrane pore radius of 0.68 nm. M4 possessed an MWCO value of 777 ± 29 g mol^{-1} (corresponding to the pore radius of 0.81 nm), which was larger than those of M2 and M3. Accordingly, methanol permeance for M2 (9.8 L m^{-2} h^{-1} bar^{-1}) was higher than that for M3 (5.9 L m^{-2} h^{-1} bar^{-1}) and M4 was 7.7 L m^{-2} h^{-1} bar^{-1}.

The relations between the physical properties and OSN performance of membranes are shown in Fig. 4c. The interplay between membrane pore size, density, and thickness resulted in various molecular transport mechanisms (Figs. 4d–4f). Although M2 had a medium pore size (r = 0.72 nm) and medium thickness (81.6 μm), it exhibited medium MWCO (624 ± 27 g mol^{-1}) with the highest permeance (9.8 L m^{-2} h^{-1} bar^{-1}) due to its lowest membrane density (0.58 g cm^{-3}). Thus, pore size was the main contributing factor for MWCO, but permeance was mainly influenced by membrane density. A low membrane density indicated that the membrane contained highly interconnected free volume, which provided many channels for the facile transport of solvent molecules as illustrated in Fig. 4d. By increasing the membrane density (0.76 g cm^{-3}) while reducing the pore size (r = 0.68 nm), as in the case of M3, a membrane with the lowest MWCO (553 ± 27 g mol^{-1}) and the lowest permeance (5.9 L m^{-2} h^{-1} bar^{-1}) can be obtained, although M3 was the thinnest membrane (50.6 μm). Moreover, these observations support the argument that pore size mainly controlled the MWCO and membrane density mainly governed the permeance. A high density indicated that the membrane contained many unconnected free volumes which, in combination with small pore size, hampered molecular transport (Fig. 4e). M4 had inhomogeneous pore sizes, as shown in SEM and AFM images (Fig. 3d and 3l). The solute rejection will be governed by the largest pore size, whereas the permeance will be determined by the total number of available channels (Fig. 4f). M4 exhibited the largest pore size (r = 0.81 nm) with a medium density of 0.64 g cm^{-3}; thus, it showed the largest MWCO with medium permeance (7.7 L m^{-2} h^{-1} bar^{-1}) because it had a few large channels with many unconnected free volumes.

The permeance and solvent parameters of M2–M4 exhibited a linear relation (Fig. 4g). In general, M2 exhibited the highest permeance for any tested solvent, followed by M4 and M3. These results were in line with the previous observations (Fig. 4d–f), where membrane density primarily affected the permeance. Furthermore, solvent polarity was proportional to the solvent permeance (Fig. 4h); the high-polarity

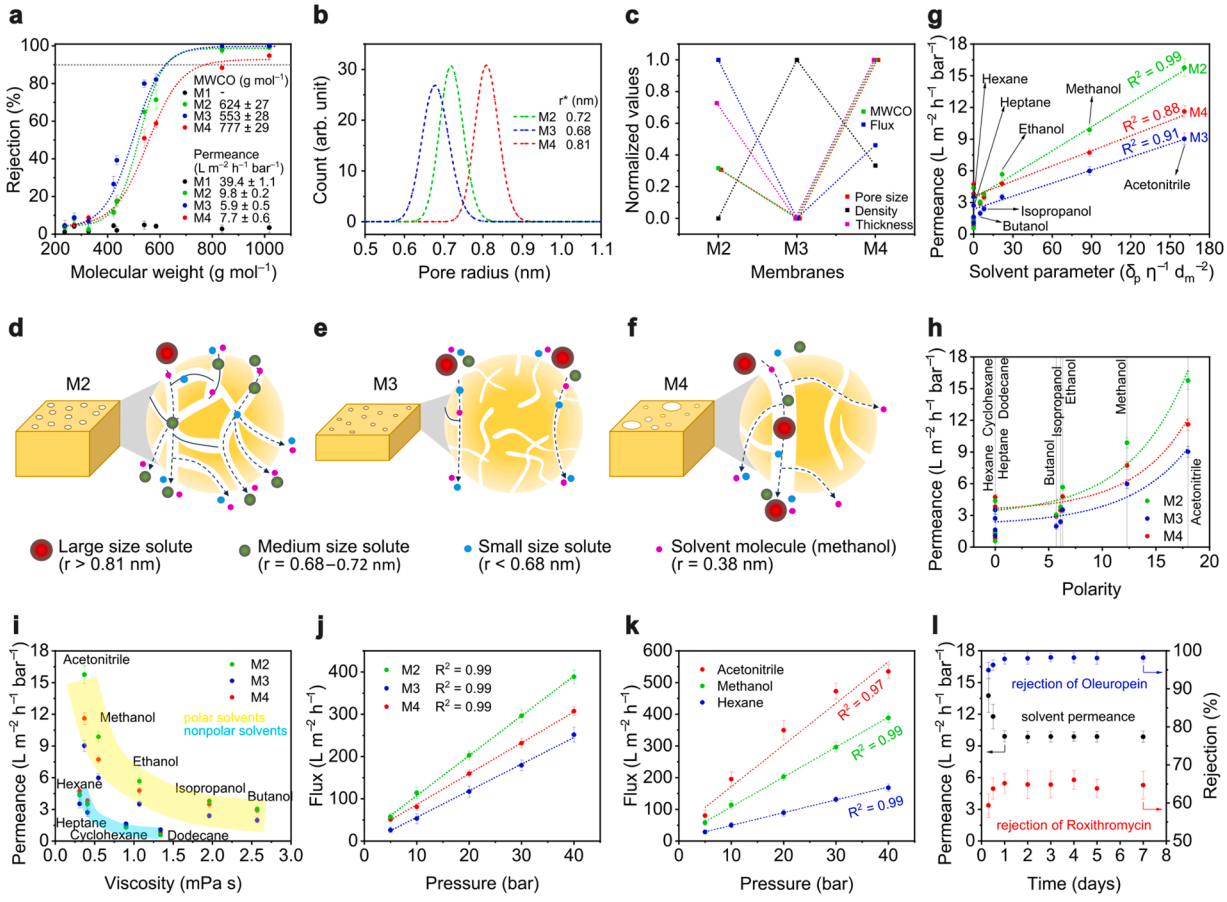

Fig. 4. Rejection (a) and pore size distribution (b) curves for M1–M4; correlation graph between membrane physical properties and performances (c); schematic of the proposed membrane morphologies and molecular transport mechanism in M2 (d), M3 (e), and M4 (f); effects of solvent parameter (g), solvent polarity (h), and solvent viscosity (i) on the permeance; methanol flux through M2, M3, and M4 at different applied pressures (j); acetonitrile, methanol, and hexane fluxes through M2 at different applied pressures (k); OSN long-term stability of M2 (l); all nanofiltration measurements were conducted in methanol at 20 °C and 30 bar unless otherwise stated.

solvents had a high permeance. These findings indicated that since the P(BiL$^{=}$)$_{ROP}$ membranes were hydrophilic, the membranes had better wetting degrees with polar solvents, facilitating faster flow and resulting in higher permeance. These observations were also supported by previously reported studies (Miao et al., 2020; Xu et al., 2012). As expected, the solvent viscosity (for both polar and non-polar solvents) was inversely proportional to the solvent permeance (Fig. 4i) because higher-viscosity solvents had higher transport resistance, as demonstrated by the Hagen-Poiseuille equation (Eq. S2). Two trends were clearly observed in Fig. 4i, where polar solvents exhibited higher permeance than non-polar solvents. The methanol flux linearly increased with the applied pressure (Fig. 4j), indicating the mechanical stability of membranes under high pressures and the absence of concentration polarization that could reduce the permeance. For other solvents, such as acetonitrile and hexane, the linearity between applied pressure and solvent permeance remained observed (Fig. 4k). These observations suggest that the solvent properties (polarity, molecular size, and viscosity) did not alter the mechanical stability of the membranes. The solvent properties only affect the magnitude of the permeance through the membrane. As M2 exhibited the most optimized OSN performance with the highest flux and medium MWCO, it was further tested for long-term nanofiltration stability over a 1-week continuous OSN test (Fig. 4l). During the first 24 h, the methanol permeance slightly decreased from 13.7 to 9.9 L m^{-2} h^{-1} bar^{-1} because of membrane stabilization. After 24 h, the membrane exhibited stable permeance during the 1 week. Accordingly, roxithromycin (molecular weight: 837.05 g mol^{-1}) and oleuropein (molecular weight: 540.51 g mol^{-1}) rejections slightly increased from 59.4% to 65.4% and from 94.9% to 97.8%, respectively. After the initial tightening of the membrane, it exhibited stable rejections of both solutes for 1 week.

3. Conclusion

Recyclable nanofiltration membranes were successfully fabricated from P(BiL$^{=}$)$_{ROP}$ and P(BiL$^{=}$)$_{ROMP}$ polymers using γ-butyrolactone as a green solvent. These polymers were obtained from a single monomer (BiL$^{=}$) and can be depolymerized into the parent monomer, following the unique "one monomer–two polymers–one monomer" transformation. The P(BiL$^{=}$)$_{ROP}$ membrane exhibited strong resistance toward water, heptane, hexane, acetonitrile, and various alcohols, enabling its potentials applications in various liquid media. The morphology and mechanical properties of the membranes were tunable via physical treatments (annealing, hot-pressing, and air exposure) without modifying their chemical and thermal properties. Annealing yielded membrane with a medium pore size (r = 0.72 nm), while maintaining large free volume in the cross-section, allowing for high solvent flux (9.8 L m^{-2} h^{-1} bar^{-1}). Hot-pressing induced densification in both skin layer and the cross-section, resulting in membrane with a small pore size (r = 0.68 nm) and low solvent permeance (5.9 L m^{-2} h^{-1} bar^{-1}). After exposing the cast solution to air before phase inversion, membrane with a large pore size (r = 0.81 nm) and medium solvent flux (7.7 L m^{-2} h^{-1} bar^{-1}) were obtained. Furthermore, the interplay between membrane pore size, density, thickness, and membrane nanofiltration performance was assessed. Solute rejection was mainly determined by the

pore size of membranes, whereas solvent flux was mainly affected by the membrane density that governed the free volume interconnectivity. The most optimized $P(BiL^{=})_{ROP}$ membrane (M2) demonstrated an MWCO value of 624 ± 27 g mol^{-1}, with the highest methanol permeance (9.8 L m^{-2} h^{-1} bar^{-1}). M2 also exhibited excellent long-term stability under continuous cross-flow filtration in methanol over one week. The fabrication of fully recyclable polymer nanofiltration membranes using green solvents was in line with sustainability and circular economy principles.

Statement of novelty

Herein, we have developed nanofiltration membranes based on novel fully recyclable polyester $P(BiL^{=})_{ROP}$ and poly(cyclic olefin) $P(BiL^{=})_{ROMP}$, using γ-butyrolactone as the green solvent. These polymers were synthesized from a single monomer ($BiL^{=}$) and exhibit the unique "one monomer–two polymers–one monomer" closed-loop lifecycle. These recyclable polymers enabled fabrication of membranes with distinct properties, which can be used for various applications. Thus, the results reported herein call for rapid dissemination. The depolymerizability of these novel polymers enabled the recycling of the after-used membranes, paving the way toward a sustainable and circular plastic economy.

CRediT authorship contribution statement

Rifan Hardian: Writing – original draft, Visualization, Validation, Methodology, Investigation, Formal analysis, Data curation, Conceptualization. **Abdul Ghaffar:** Data curation. **Changxia Shi:** Writing – review & editing, Methodology, Investigation, Conceptualization. **Eugene Y.-X. Chen:** Writing – review & editing, Supervision, Resources, Project administration, Methodology, Funding acquisition, Conceptualization. **Gyorgy Szekely:** Writing – review & editing, Supervision, Resources, Project administration, Methodology, Investigation, Funding acquisition, Conceptualization.

Declaration of competing interest

The authors declare that they have no known competing financial interests or personal relationships that could have appeared to influence the work reported in this paper.

Data availability

Data will be made available on request.

Acknowledgements

The research reported in this publication was supported by funding provided by the King Abdullah University of Science and Technology (KAUST). Fig. 1 and the graphical abstract were created by Ana Bigio, scientific illustrator at KAUST. The work performed at Colorado State University was supported by the U.S. Department of Energy, Office of Energy Efficiency and Renewable Energy, Advanced Materials and Manufacturing Technologies Office (AMMTO) and Bioenergy Technologies Office (BETO), through the Environment (BOTTLE) Consortium under Contract DE-AC36-08GO28308 with the National Renewable Energy Laboratory (NREL), operated by Alliance for Sustainable Energy, LLC.

Supplementary materials

Supplementary material associated with this article can be found, in the online version, at doi:10.1016/j.memlet.2024.100067.

References

Alder, C.M., Hayler, J.D., Henderson, R.K., Redman, A.M., Shukla, L., Shuster, L.E., Sneddon, H.F., 2016. Updating and further expanding GSK's solvent sustainability guide. Green Chem. 18, 3879–3890. https://doi.org/10.1039/C6GC00611F.

Belfort, G., 2019. Membrane filtration with liquids: a global approach with prior successes, new developments and unresolved challenges. Angewand. Chem. Int. Ed. 58, 1892–1902. https://doi.org/10.1002/anie.201809548.

Caretto, A., Noè, M., Selva, M., Perosa, A., 2014. Upgrading of Biobased Lactones with Dialkylcarbonates. ACS Sustain. Chem. Eng. 2, 2131–2141. https://doi.org/10.1021/sc500323a.

Cheng, X.Q., Wang, Z.X., Jiang, X., Li, T., Lau, C.H., Guo, Z., Ma, J., Shao, L., 2018. Towards sustainable ultrafast molecular-separation membranes: from conventional polymers to emerging materials. Prog. Mater. Sci. 92, 258–283. https://doi.org/10.1016/j.pmatsci.2017.10.006.

Clarke, C.J., Tu, W.-C., Levers, O., Bröhl, A., Hallett, J.P., 2018. Green and sustainable solvents in chemical processes. Chem. Rev. 118, 747–800. https://doi.org/10.1021/acs.chemrev.7b00571.

Datta, S.J., Mayoral, A., Murthy Srivatsa Bettahalli, N., Bhatt, P.M., Karunakaran, M., Carja, I.D., Fan, D., Graziane, M., Mileo, P., Semino, R., Maurin, G., Terasaki, O., Eddaoudi, M., 2022. Rational design of mixed-matrix metal-organic framework membranes for molecular separations. Science 376, 1080–1087. https://doi.org/10.1126/science.abe0192.

Dodero, A., Scarfi, S., Mirata, S., Sionkowska, A., Vicini, S., Alloisio, M., Castellano, M., 2021. Effect of crosslinking type on the physical-chemical properties and biocompatibility of Chitosan-based electrospun membranes. Polymer. (Basel) 13, 831. https://doi.org/10.3390/polym13050831.

Fatima, A., Ortiz-Albo, P., Neves, L.A., Nascimento, F.X., Crespo, J.G., 2023. Biosynthesis and characterization of bacterial cellulose membranes presenting relevant characteristics for air/gas filtration. J. Memb. Sci. 674, 121509 https://doi.org/10.1016/j.memsci.2023.121509.

Figoli, A., Marino, T., Simone, S., Nicolò, E.D., Li, X.-M., He, T., Tornaghi, S., Drioli, E., 2014. Towards non-toxic solvents for membrane preparation: a review. Green Chem. 16, 4034–4059. https://doi.org/10.1039/C4GC00613E.

Gribble, G.W., 1991. Chapter 5b - Natural products containing a cyclohexane, cyclohexene, or cyclohexadiene subunit. In: Sainsbury, M. (Ed.), Second Supplements to the 2nd Edition of Rodd's Chemistry of Carbon Compounds. Elsevier, Amsterdam, pp. 375–445. https://doi.org/10.1016/B978-044453347-0.50066-5.

Hardian, R., Cywar, R.M., Chen, E.Y.-X., Szekely, G., 2022. Sustainable nanofiltration membranes based on biosourced fully recyclable polyesters and green solvents. J. Memb. Sci. Lett. 2, 100016 https://doi.org/10.1016/j.memlet.2022.100016.

Hardian, R., Pogany, P., Lee, Y.M., Szekely, G., 2021. Molecular sieving using metal–polymer coordination membranes in organic media. J. Mater. Chem. A 9, 14400–14410. https://doi.org/10.1039/D1TA02601A.

Hessel, V., Tran, N.N., Asrami, M.R., Tran, Q.D., Long, N.V.D., Escribà-Gelonch, M., Tejada, J.O., Linke, S., Sundmacher, K., 2021. Sustainability of green solvents – review and perspective. Green Chem. https://doi.org/10.1039/D1GC03662A.

Hu, W., Wang, Z., Xiao, Y., Zhang, S., Wang, J., 2019. Advances in crosslinking strategies of biomedical hydrogels. Biomater. Sci. 7, 843–855. https://doi.org/10.1039/C8BM01246F.

Kim, D., Nunes, S.P., 2021. Green solvents for membrane manufacture: recent trends and perspectives. Curr. Opin. Green. Sustain. Chem. 28, 100427 https://doi.org/10.1016/j.cogsc.2020.100427.

Lee, J.W., Han, M.-S., Choi, S., Yi, J., Lee, T.W., Lee, S.Y., 2011. 3.15 - Organic Acids: succinic and Malic Acids. In: Moo-Young, M. (Ed.), Comprehensive Biotechnology, 2nd Edition. Academic Press, Burlington, pp. 149–161. https://doi.org/10.1016/B978-0-08-088504-9.00183-5.

Li, B., Wang, S., Loh, X.J., Li, Z., Chung, T.-S., 2023. Closed-loop recyclable membranes enabled by covalent adaptable networks for water purification. Proceed. Natl. Acad. Sci. 120, e2301009120 https://doi.org/10.1073/pnas.2301009120.

Miao, A., Wei, M., Xu, F., Wang, Y., 2020. Influence of membrane hydrophilicity on water permeability: an experimental study bridging simulations. J. Memb. Sci. 604, 118087 https://doi.org/10.1016/j.memsci.2020.118087.

Nguyen Thi, H.Y., Nguyen, B.T.D., Kim, J.F., 2021. Sustainable fabrication of organic solvent nanofiltration membranes. Membranes 11, 19. https://doi.org/10.3390/membranes11010019.

Nunes, S.P., Culfaz-Emecen, P.Z., Ramon, G.Z., Visser, T., Koops, G.H., Jin, W., Ulbricht, M., 2020. Thinking the future of membranes: perspectives for advanced and new membrane materials and manufacturing processes. J. Memb. Sci. 598, 117761 https://doi.org/10.1016/j.memsci.2019.117761.

Ogunmakinde, O.E., Egbelakin, T., Sher, W., 2022. Contributions of the circular economy to the UN sustainable development goals through sustainable construction. Resour. Conserv. Recycl. 178, 106023 https://doi.org/10.1016/j.resconrec.2021.106023.

Rasool, M.A., Vankelecom, I.F.J., 2021. Preparation of full-bio-based nanofiltration membranes. J. Memb. Sci. 618, 118674 https://doi.org/10.1016/j.memsci.2020.118674.

Rebers, L., Reichsöllner, R., Regett, S., Tovar, G.E.M., Borchers, K., Baudis, S., Southan, A., 2021. Differentiation of physical and chemical cross-linking in gelatin methacryloyl hydrogels. Sci. Rep. 11, 3256. https://doi.org/10.1038/s41598-021-82393-z.

Serbanescu, O.S., Voicu, S.I., Thakur, V.K., 2020. Polysulfone functionalized membranes: properties and challenges. Mater. Today Chem. 17, 100302 https://doi.org/10.1016/j.mtchem.2020.100302.

Shi, C., Clarke, R.W., McGraw, M.L., Chen, E.Y.-X., 2022. Closing the "One Monomer–Two Polymers–One Monomer" Loop via Orthogonal (De)polymerization

of a Lactone/Olefin Hybrid. J. Am. Chem. Soc. 144, 2264–2275. https://doi.org/10.1021/jacs.1c12278.
Sholl, D.S., Lively, R.P., 2016. Seven chemical separations to change the world. Nature 532, 435–437. https://doi.org/10.1038/532435a.
Strivens, T.A., 1999. 14 - An introduction to rheology. In: Lambourne, R., Strivens, T.A. (Eds.), Paint and Surface Coatings (Second Edition), Woodhead Publishing Series in Metals and Surface Engineering. Woodhead Publishing, pp. 550–574. https://doi.org/10.1533/9781855737006.550.
Syeda, S.R., Khan, E.A., Padungwatanaroj, O., Kuprasertwong, N., Tula, A.K., 2022. A perspective on hazardous chemical substitution in consumer products. Curr. Opin. Chem. Eng. 36, 100748 https://doi.org/10.1016/j.coche.2021.100748.
Tan, Z., Chen, S., Peng, X., Zhang, L., Gao, C., 2018. Polyamide membranes with nanoscale Turing structures for water purification. Science 360, 518–521. https://doi.org/10.1126/science.aar6308.
Tomietto, P., Russo, F., Galiano, F., Loulergue, P., Salerno, S., Paugam, L., Audic, J.-L., De Bartolo, L., Figoli, A., 2022. Sustainable fabrication and pervaporation application of bio-based membranes: combining a polyhydroxyalkanoate (PHA) as biopolymer and Cyrene™ as green solvent. J. Memb. Sci. 643, 120061 https://doi.org/10.1016/j.memsci.2021.120061.
Tran, D.H., Ulbricht, M., 2023. Cellulose-cellulose composite membranes for ultrafiltration. J. Memb. Sci. 672, 121426 https://doi.org/10.1016/j.memsci.2023.121426.
Xie, W., Li, T., Tiraferri, A., Drioli, E., Figoli, A., Crittenden, J.C., Liu, B., 2021. Toward the next generation of sustainable membranes from green chemistry principles. ACS Sustain. Chem. Eng. 9, 50–75. https://doi.org/10.1021/acssuschemeng.0c07119.
Xu, Q., Yang, Y., Wang, X., Wang, Z., Jin, W., Huang, J., Wang, Y., 2012. Atomic layer deposition of alumina on porous polytetrafluoroethylene membranes for enhanced hydrophilicity and separation performances. J. Memb. Sci. 415–416, 435–443. https://doi.org/10.1016/j.memsci.2012.05.031.
Yang, C., Cavalcante, J., Bastos de Freitas, B., Lauersen, K.J., Szekely, G., 2023. Crude algal biomass for the generation of thin-film composite solvent-resistant nanofiltration membranes. Chem. Eng. J. 470, 144153 https://doi.org/10.1016/j.cej.2023.144153.
Zakharova, M., Tibbe, M.P., Koch, L.S., Le-The, H., Leferink, A.M., van den Berg, A., van der Meer, A.D., Broersen, K., Segerink, L.I., 2021. Transwell-integrated 2 μm thick transparent polydimethylsiloxane membranes with controlled pore sizes and distribution to model the blood-brain barrier. Adv. Mater. Technolog. 6, 2100138 https://doi.org/10.1002/admt.202100138.
Zou, D., Nunes, S.P., Vankelecom, I.F.J., Figoli, A., Lee, Y.M., 2021. Recent advances in polymer membranes employing non-toxic solvents and materials. Green Chem. 23, 9815–9843. https://doi.org/10.1039/D1GC03318B.